Check for updates

Zinc gluconate as a multifunctional electrolyte additive for dendrite-free and long-life zinc ion batteries

Yaling Ji,[a] Ronghan Jiang,[a] Xiqing Mai,[a] Xueqin Zhang,[a] Song Lu, [ID][a] Xusheng Wang, [ID][b] Min Guo,[a] Jiadi Ying,[a] Qi Shen, [ID][a] Yeqing Wang, [ID][a] Zhixin Yu [ID][c] and Tiancun Liu [ID]*[a]

Aqueous zinc ion batteries (AZIBs) have attracted much attention owing to their low cost, high capacity and superior safety, but dendrite growth, hydrogen evolution and corrosion reaction hinder their applications. Herein, zinc gluconate (ZG) is introduced as an effective additive to the frequently used $ZnSO_4$ electrolyte in AZIBs. Particularly, there are rich oxygen-containing functional groups in ZG, such as hydroxyl groups, which can promote the preferential ZG adsorption and subsequent dispersion of zinc ions on the electrode interface. Consequently, partially concentrated zinc metal electroreduction can be well suppressed, and the hydrogen evolution reaction (HER) and fatal corrosion are also effectively alleviated due to the isolation of free water and sulfate anions. In addition, ZG addition improves the electrochemical properties of AZIBs. Symmetric zinc batteries achieve ultra-long and stable capabilities of over 3200 h and 1000 h at 1 mA cm^{-2} (1 mAh cm^{-2}) and 3 mA cm^{-2} (3 mAh cm^{-2}), respectively. Asymmetric cells exhibited an ultra-high average coulombic efficiency of 99.8% for 400 cycles at 5 mA cm^{-2} and 3 mAh cm^{-2}. The full battery using $NH_4V_4O_{10}$ exhibits excellent cycling stability and higher capacity retention. This study can provide a reference for developing highly stable electrolytes for AZIBs.

1. Introduction

Lithium-ion batteries, which currently occupy the main market in the portable energy storage field, have hindered their application in large-scale energy storage due to the rising cost caused by limited lithium resources.[1,2] In addition, the use of toxic and flammable organic electrolytes poses safety risks, such as fire and explosion.[3,4] Moreover, the safety of people's lives and property is threatened. In contrast, aqueous zinc-ion batteries (AZIBs) are considered one of the most promising systems for grid energy storage because of their inherent low cost (about one-sixth of the price of lithium-ion batteries), high safety and outstanding environmental friendliness.[5–7] In particular, zinc metal anodes possess great advantages, such as rich natural resources, high theoretical capacity (820 mAh g^{-1} and 5851 mAh cm^{-3}), low redox potential (−0.76 V *vs.* standard hydrogen electrode), non-toxicity,

and a non-flammable retardant nature.[8–10] However, the low coulombic efficiency (CE), serious zinc dendrite growth, hydrogen evolution reaction (HER) and corrosion side reactions greatly limit the practical application of the zinc metal anode and the industrialization or commercialization of related AZIBs.[11–14] First, due to the inherent defects of the zinc foil, inhomogeneous distribution of the electric field and zinc ions during the process of zinc electroreduction inevitably induces uneven zinc deposition and occurrence of the tip effect, which greatly promotes the growth of notorious zinc dendrites and punctures the separator, thus leading to short circuit and battery failure. Second, because the zinc metal anode is thermodynamically unstable in the weakly acidic zinc salt electrolyte, side reactions such as HER and corrosion inevitably occur, which greatly limits the stability of the zinc metal anode. Therefore, there is an urgent need to develop effective methods for solving these problems.

To handle these intractable issues, various studies have been reported on the inhibition of dendrite growth and alleviation of HER and corrosion reactions, mainly including electrode design,[15–17] protective coating construction,[18–22] separator preparation[23–25] and electrolyte modification.[26–30] However, the optimization procedures for zinc anodes and substrates are generally complex and expensive. In contrast, among these strat-

[a]Institute of New Energy, School of Chemistry and Chemical Engineering, Shaoxing University, Zhejiang, Shaoxing 312000, China
[b]School of Materials Science and Engineering, Zhejiang Sci-Tech University, Hangzhou 310018, China
[c]Department of Energy and Petroleum Engineering, University of Stavanger, 4036 Stavanger, Norway. E-mail: liutc@usx.edu.cn

egies, the electrolyte modification approach is relatively simple, involves the use of various additives, and is an efficient and feasible method for stabilizing AZIBs. Electrolyte additives generally exhibit a strong binding affinity with zinc ions, effectively inducing uniform dispersion and nucleation of ions. This process promotes homogeneous zinc deposition while simultaneously modifying the solvation sheath structure to suppress the activity of free water. Through these mechanisms, electrolyte additives can significantly inhibit HER, corrosion reactions and other side reactions occurring at the interface, thereby enhancing the overall stability and cycling performance of zinc metal anodes.[31–33] In particular, organic additives have been utilized to advance the stability, such as the silk peptide,[34] phenylalanine,[35] N-acetyl-ε-caprolactam,[36] melamine,[37] sorbitol,[38] nicotinic acid,[39] ethanol[40] and butyrolactam.[41] Similarly, inorganic additives, such as soluble salts,[42–44] nanoparticle additives[45,46] and small-sized nanosheets,[47,48] have also been applied to extend the working lifespan of AZIBs. Although these additives play a significant role in improving battery performance, most of the reported additives are toxic or difficult to apply on a large scale, which greatly influences the environmentally friendly advantage and low cost of AZIBs. In addition, this may delay the practical application and commercialization of AZIBs, which are urgently required for large-scale energy storage. Therefore, it is of great significance to develop a low-cost, efficient and non-toxic electrolyte additive to improve the stability and usability of AZIBs.

In this study, we develop a cheap and accessible zinc gluconate (ZG) as a functional electrolyte additive to modify the zinc sulfate electrolyte and optimize the electrode interface. It has been reported that polar groups, such as amino or hydroxyl groups, can facilitate the attraction of zinc ions. In particular, there are rich oxygen-containing functional groups in ZG, such as the hydroxyl group. ZG molecules can preferentially adsorb onto the zinc anode surface. Simultaneously, they modulate the solvation structure, inhibit the activity of free water, optimize the electrode/electrolyte interface, resist the attack of free water by shielding the surface, and facilitate the nucleation of zinc ions and their homogeneous dispersion. Subsequently, dendritic zinc development and derivative side reactions of the HER and corrosion behavior on the electrode interface are effectively relieved. Therefore, based on the above advantages, it is vital to modify the electrolyte by adding ZG, enhance the stable zinc deposition/dissolution and prolong the performances of AZIBs. As a result, symmetric cells with the ZG additive achieve an extremely superior demonstration of stable cycling of over 3200 h under conditions of 1 mA cm^{-2} and 1 mAh cm^{-2}, and an ultra-high average CE of 99.8% can also be achieved in asymmetric cells for 400 cycles at 5 mA cm^{-2} and 3 mAh cm^{-2}. Compared to the pristine electrolyte, the full cell using ZG shows a more excellent cycling stability and reversibility.

2. Results and discussion

Fig. 1a shows the long-time cycling stability of symmetric cells using different electrolytes at a current density of 1 mA cm^{-2}

and an areal capacity of 1 mAh cm^{-2}. It can be clearly observed that the presence of the ZG additive effectively improves the stability of the zinc metal anode. Meanwhile, it should be pointed out that an additional amount of ZG in the electrolyte exerts an impact on the lifespan performance of cells. In particular, when the concentration of the additive is selected at 10 mM, the symmetric cell displays the longest cycling performance of 3200 h, which is notably superior to other electrolytes. A uniform interface adsorption layer cannot be produced at an insufficient additive concentration of 5 mM, resulting in weak effects. However, excess adsorption would increase the transfer barrier of zinc ions on the electrode interface as the concentration exceeds the appropriate condition, which may not be conducive to facilitating the uniformity of zinc ion distribution. As shown in Fig. S1, when the addition amount exceeds 10 mM and increases to 50 mM or 100 mM, the ionic conductivity subsequently decreases, which should be caused by the increased energy barrier of ionic transport due to excessive ZG accumulation on the electrode interface. Therefore, an electrolyte with an additive amount of 10 mM is considered the main research object in this work, which is named ZSO–ZG. Fig. 1b and c display scanning electron microscopy (SEM) images of cycled zinc electrodes after 50 plating/stripping cycles in ZSO–ZG and ZSO electrolytes, respectively. In particular, for zinc foil in ZSO–ZG, there is a relatively flat surface morphology and reduced gap appearance, which should be caused by the effective suppression of corrosion behavior and the orderly guidance of zinc deposition.[49] In contrast, the zinc electrode in the pristine ZSO electrolyte shows a rather heterogeneous zinc growth behavior accompanied by the production of by-products.

To further verify the improved deposition procedure induced by the ZG additive, real-time optical observation is implemented using a self-made device. As shown in Fig. 1d and e, the electrode morphology during Zn plating at 10 mA cm^{-2} is exhibited. Fig. 1d displays detailed behavior in ZSO–ZG, from which a dendrite-free electrode surface and avoided HER can be obtained even after 45 min due to the abilities of inducing zinc dispersion and isolating free water. In contrast, as shown in Fig. 1e, three distinct small bubbles (marked by red circles) are visible near the Zn metal anode surface, while the plating time was only 15 min, indicating that HER is triggered. Then, a small metal protrusion (pointed by the red box) can be clearly noticed from the zinc substrate, while the plating time extends to 30 min. As the process continues for 45 min, uneven zinc deposition and dendrite growth become even more obvious. The comparison difference further reflects the significant effects of regulating homogenous zinc deposition behavior and suppressing interfacial hydrogen evolution and precipitation due to ZG introduction. In brief, Fig. 1f schematically illustrates the action process of zinc deposition between these two electrolytes. Because of the deficient capacity of dispersing zinc ions and defending free water on the electrode interface, inevitable dendrite formation and competitive HER still exist in pristine ZSO, producing other side reactions and shortening the electrode lifespan. In sharp contrast, functional ZG additive tends to preferentially adsorb on
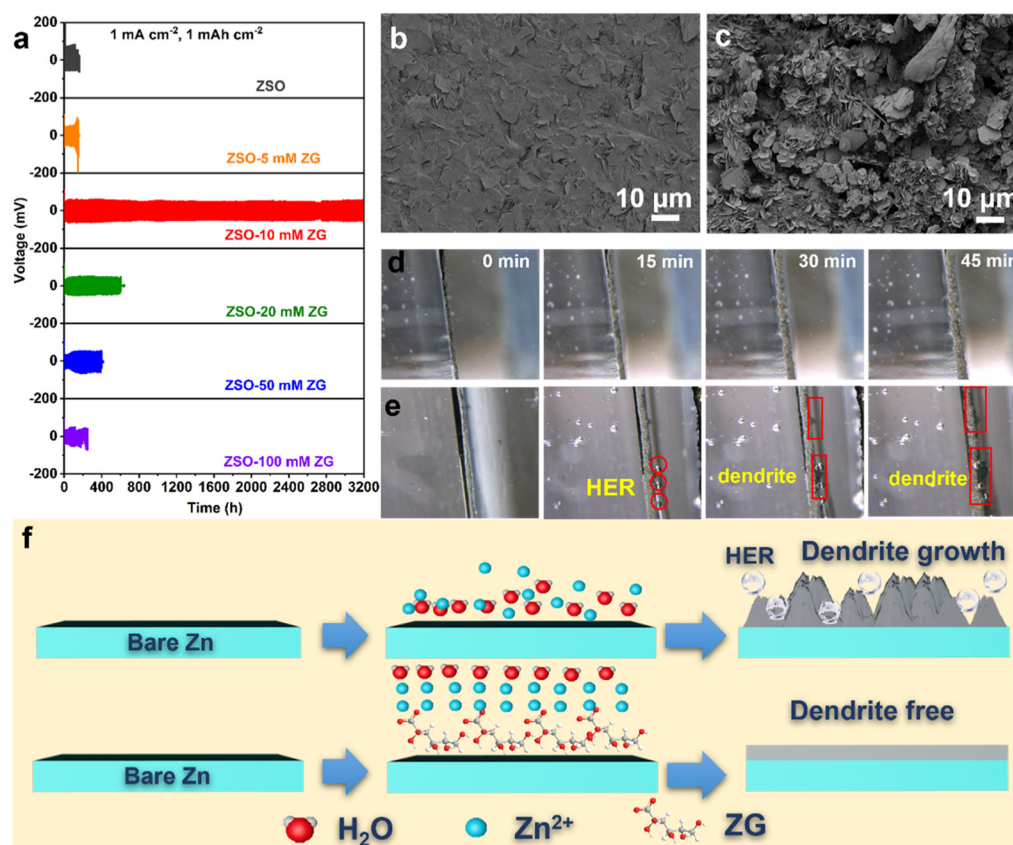
Fig. 1 (a) Comparative cycling performance of the symmetric cells in different electrolytes at 1 mA cm^{-2}. SEM images of the cycled zinc foil in (b) ZSO–ZG and (c) ZSO at 2 mA cm^{-2} for 50 cycles. The real-time optical images of zinc plating at 10 mA cm^{-2} in (d) ZSO–ZG and (e) ZSO. (f) The schematic of zinc plating and growth in ZSO and ZSO–ZG electrolytes.

the zinc surface, which is beneficial to attracting zinc ions, guiding orderly dispersion and avoiding local accumulation. Therefore, the tip effect and dendrite growth will be effectively suppressed. Meanwhile, the adsorption layer of ZG molecular blocks the attack of free water on the electrode interface and alleviates the corrosion behavior, and SO$_4^{2-}$ anions are rejected; thus, the formation of by-products (Zn$_4$(OH)$_6$SO$_4$·xH$_2$O, ZHS) can be inhibited.

To investigate the effects of ZG additive introduction on electrolyte physicochemical properties, a series of characterization studies were conducted. First, the pH test results show a slight increase caused by ZG additives in the ZSO electrolyte (Fig. S2); this is because the introduction of ZG can suppress the dissociation of free water. However, individual pH changes cannot achieve performance improvement, which can be determined, as shown in Fig. 1a. Meanwhile, wettability exploration of the two electrolytes is compared using contact angle measurements, from which the ZSO–ZG electrolyte can achieve a contact angle of approximately 89°, which is lower than the 94° of pristine ZSO (Fig. S3). This difference may be attributed to the ZG molecular component disrupting internal hydrogen bonding interactions and reducing the surface tension of the functional electrolyte. The electrostatic potential (ESP) distribution of the ZG molecule is illustrated in Fig. 2a, from which

the charge enrichment appears near oxygen-containing groups, indicating that these sites are beneficial for attracting and coordinating zinc ions. Furthermore, DFT analysis was employed to evaluate preferential adsorption between H$_2$O and the ZG molecule. As displayed in Fig. 2b, the calculated results reveal that the ZG molecule exhibits larger adsorption energy compared to H$_2$O molecules on both the zinc (002) and (101) crystal planes, demonstrating that ZG can achieve preferential adsorption on the zinc surface. The corresponding molecular models for adsorption are depicted in Fig. S4. This effectively promotes the existence of a shielding layer on the interface, which may help isolate the contact of free water and sulfate anions with the zinc electrode, thereby mitigating corrosion issues. Similarly, preferential ZG adsorption facilitates zinc ion dispersion and avoids nucleation concentration.[50] To investigate the interfacial migration kinetics of zinc ions, electrochemical impedance spectroscopy (EIS) was conducted at various temperatures for the two electrolytes (Fig. 2c and S5). By fitting the result relationship between impedance and temperature, it can be found that the activation energy of the cell using ZSO–ZG electrolyte (24.03 kJ mol^{-1}) is lower than that of pristine ZSO (29.34 kJ mol^{-1}), indicating a low energy barrier for zinc ion migration at the interface and then facilitating rapid zinc transfer. Moreover, zinc ion transfer number
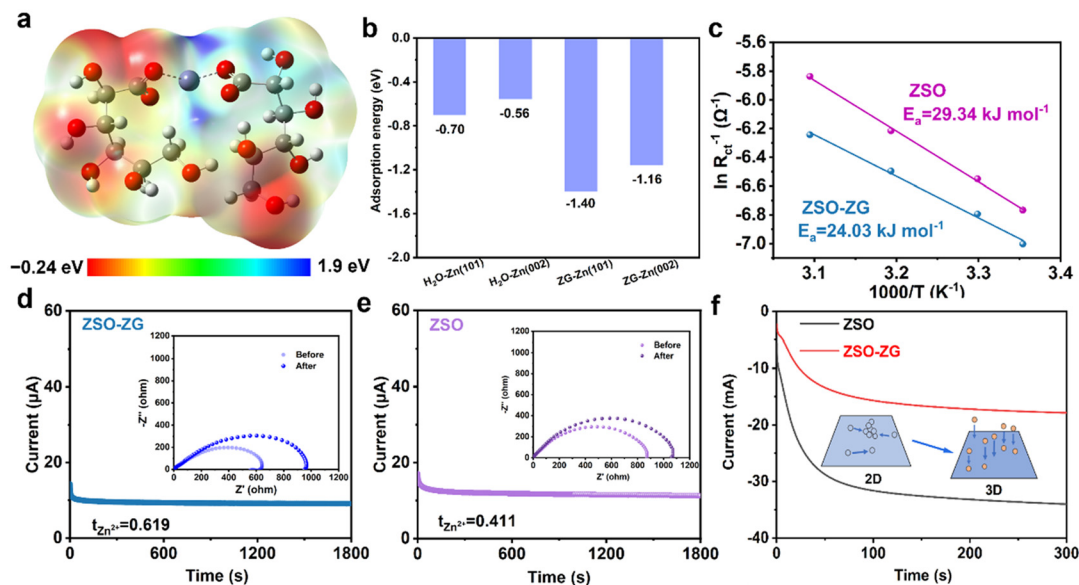
Fig. 2 (a) ESP mapping of the ZG molecule. (b) Adsorption energy of the H_2O and ZG components on Zn (002) and Zn (101) planes. (c) Arrhenius curves and calculated activation energies of the symmetric cells using two electrolytes. The constant current polarization curves and Nyquist plots before/after polarization in (d) ZSO–ZG and (e) ZSO electrolytes. (f) CA curves.

measurements in ZSO and ZSO–ZG have also been obtained by conducting EIS curves and constant-current polarization curves, as shown in Fig. 2d and e. Notably, the ZSO–ZG electrolyte performs a significantly higher transfer number (0.619) compared to ZSO (0.411), demonstrating that the ZG additive can accelerate zinc ion migration kinetics. It is well known that the diffusion tendency of zinc ions and the initial nucleation process exert significant effects on the subsequent deposition process. The chronoamperometry (CA) curves collected at a fixed overpotential of −150 mV were carried out to evaluate the diffusion behavior of zinc ions and changes on the zinc electrode surface. As shown in Fig. 2f and S6, the current density gradually increases in the ZSO electrolyte, which represents a continuous two-dimensional (2D) diffusion process that induces constant accumulation near the zinc tip and uneven deposition.[51] Finally, the negative deposition evolves into dendrite status and leads to short-circuit failure. In contrast, a smaller value of current density is displayed in ZSO–ZG, and the related change slows down and remains stable after 100 s, indicating that 2D diffusion behavior can be significantly inhibited. This phenomenon stems from the adsorption of zinc ions on the electrode surface, which creates a favorable environment that effectively suppresses disordered 2D diffusion. For other ZG-based electrolytes, an excessive addition concentration prolongs the disordered two-dimensional diffusion time, impeding the homogenization of the initial zinc nucleation. It should be confirmed that the ZG additive facilitates the uniform diffusion of zinc ions and the initial nucleation. Therefore, owing to uniform initial zinc nucleation, dendrite-free zinc deposition can be achieved.

Under the weak acidic conditions of the common ZSO electrolyte, corrosion behavior seriously restricts the stability of

the zinc metal electrode. To evaluate HER activity in the prepared electrolytes, linear sweep voltammetry (LSV) measurements were carried out. As shown in Fig. 3a, the HER potential of the ZSO–ZG electrolyte is obviously lower than that of pristine ZSO, indicating the improvement of reliving the attack of free water, which helps enhance a certain inhibitory effect on HER during the zinc plating/stripping process. To further investigate the corrosion behavior of the zinc electrode in the electrolytes with ZG additive, Tafel tests and immersion experiments are also conducted. Fig. 3b illustrates the Tafel results measured using a three-electrode system, from which there is a slight increase in the corrosion potential in ZSO–ZG compared to ZSO. This comparison demonstrates the mitigation effect of the ZG additive in reducing the formation of by-products and hydrogen sedimentation on the zinc metal anode. XRD patterns of the zinc foil after soaking for 7 days notably show that peaks located at 16°, 24°, and 32° correspond to significant by-product (ZHS) reduction after ZG introduction (Fig. 3c), but these peaks can still be found in pristine ZSO. As displayed in Fig. 3d–f, related SEM results further demonstrate detailed interface changes in these samples. Compared to processed zinc covered by uneven corrosion sheets in ZSO, there is a relatively small amount of sheet corrosion by-products on the zinc sample soaked in electrolyte containing ZG additive although they are not as flat as uncycled zinc foil.

In addition to side reactions, such as HER and corrosion behavior, the production of dead zinc and the resulting low CE also hinder the stable cycling of AZIBs. Therefore, asymmetric cells were assembled to conduct a series of electrochemical tests. As shown in Fig. 4a, CE tests of asymmetric cells at 5 mA cm^{-2} with an area capacity of 3 mAh cm^{-2} indicate a significant effect of the ZG additive on improving cycling stability
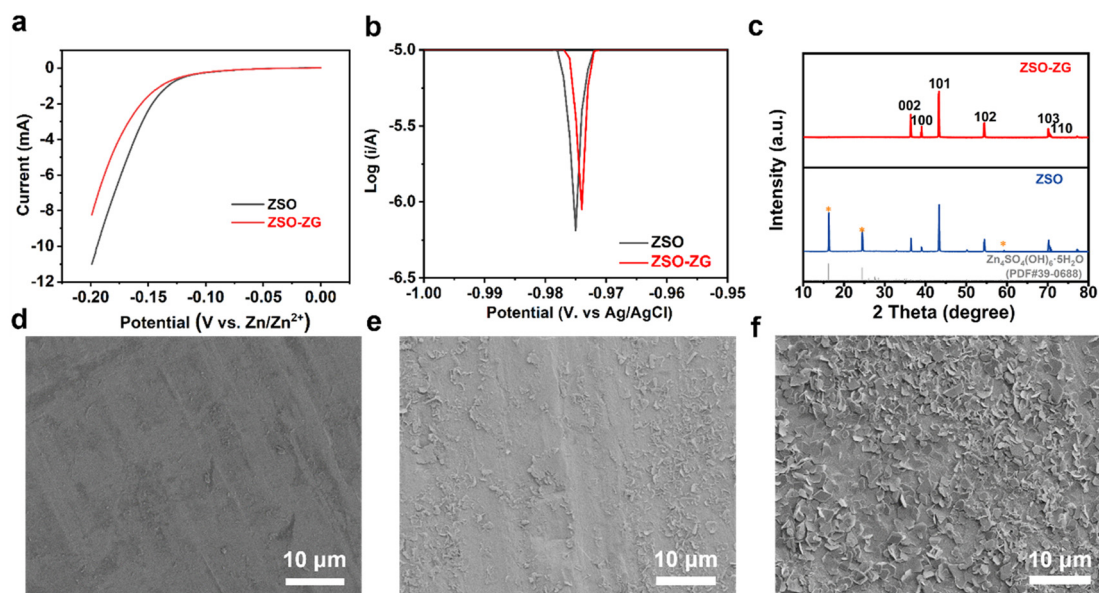
Fig. 3 (a) LSV curves of the two electrolytes. (b) Tafel plots. (c) XRD patterns of the zinc foils immersed in ZSO–ZG and ZSO after 7 days. SEM images of (d) the bare zinc foil and zinc foils immersed in the electrolytes of (e) ZSO–ZG and (f) ZSO for 7 days.
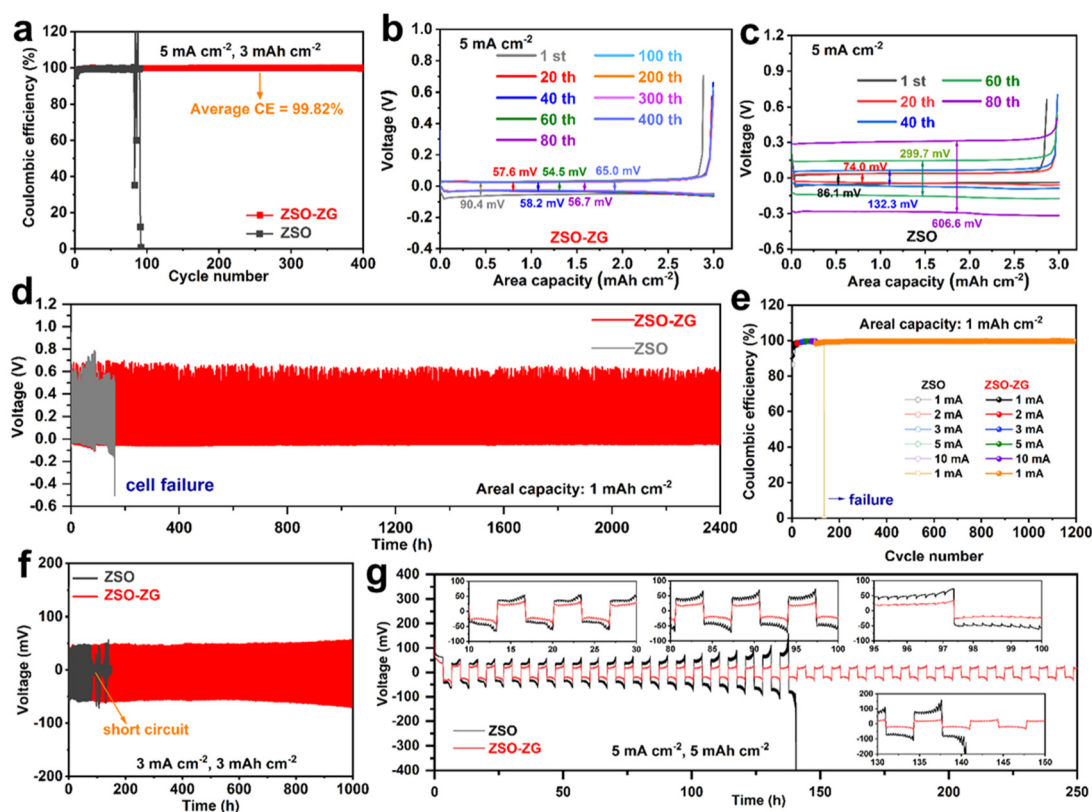
Fig. 4 (a) CE performance of the asymmetric cell in different electrolytes at 5 mA cm^{-2}. Corresponding voltage profiles at different cycles of (b) ZSO–ZG and (c) ZSO. (d) Time-voltage profiles in the rate performance of two electrolytes and (e) the corresponding rate CE comparison. (f) Cycling performance of the symmetric cells in different electrolytes at 3 mA cm^{-2}. (g) GITT results of the cells at 5 mA cm^{-2}.

and increasing the utilization ratio of zinc deposition. In particular, the asymmetric cell shows a long cycling life exceeding 400 cycles, higher initial CE (96.2% *vs.* 95.5%, Fig. S7), and maintains an average CE over 99.8%, while the cell in the ZSO electrolyte encounters a sudden failure after 80 cycles. Otherwise, corresponding voltage curves at different cycles can also be used to further assess the plating/stripping behavior of deposited zinc metals in different electrolytes. As observed from the results in ZSO–ZG, the voltage hysteresis between plating and stripping stages always remains relatively stable (Fig. 4b), with little difference in the calculated values at different cycles, from the initial 90.4 mV to 58.2 mV (100th cycle), 56.7 mV (300th cycle) and final 65.0 mV (400th cycle), indicating positive effects of stabilizing Zn plating/stripping process and reducing interfacial side reactions.[52] However, for the cell using ZSO electrolyte, a continuous increase in voltage hysteresis occurs due to the inevitable development of dead Zn and interfacial passivation layer (Fig. 4c). Specifically, a low value of 86.1 mV (1st cycle) rapidly changes to 132.3 mV (40th cycle) and then an extremely high value of 606.6 mV at the 80th cycle. This obvious variation should be explained by the confirmation of the electrode morphology in the ZSO electrolyte, as shown in Fig. 1c. In addition, rate testing results of cells at various current densities (1, 2, 3, 5 and 10 mA cm^{-2}) also show the good effect of the ZG additive. In the ZSO–ZG electrolyte, the cell maintains an ultralong cycling life for more than 2400 h, and a rapid failure only after 160 h happens in ZSO (Fig. 4d). Notably, as shown in Fig. 4e, a detailed comparison of the CE performances of the two cells further highlights the effective capabilities of reducing and even suppressing the by-products on the zinc electrode interface, which also manifests an avoided appearance of locally concentrated zinc growth.

The assembled symmetric zinc cell in ZSO–ZG also shows a good cycling stability (Fig. 4f and S8). ZG molecules can preferentially adsorb on the surface of the zinc anode, which increases interfacial transfer impedance, thereby increasing nucleation overpotential and voltage hysteresis. When working at a current density of 3 mA cm^{-2} and an areal capacity of 3 mAh cm^{-2}, a longer cycling life of 1000 h in the cell containing ZG is obtained, which is 10 times longer than the cell using ZSO (about 83 h). Even cycled at a higher current density of 10 mA cm^{-2} and higher depth of discharge (DOD) values of 10%, 17%, and 33%, the symmetric cell using ZSO–ZG can perform a longer cycling life as well (Fig. S8). Similarly, as shown in Fig. S9, the cell at different current densities (1, 2, 3, 5, and 10 mA cm^{-2}) also exhibits superior rate capability due to ZG addition. In electrolytes containing ZG additives, a smaller voltage hysteresis change can be maintained along with a stable cycling life, which is attributed to enhanced corrosion inhibition and relived by-product (insulated ZHS) formation, while the cell using ZSO encounters a short circuit failure only after about 170 h. In particular, the ZG additive can be further proved by employing the galvanostatic intermittent titration technique (GITT) to determine the positive effects of stabilizing the interface and suppressing corrosion (Fig. 4g). During the continuous plating/stripping process, a temporary charge/discharge suspension exacerbates the formation of corrosion products, thereby further shortening the stability and lifespan of the cell. Compared to the merely unchanged cycling tendency, the cell using ZSO suddenly encounters a sharp increase in voltage hysteresis after 135 h, which is mainly caused by the severe accumulation of insulated ZHS that blocks ion and electron transfer.

In order to evaluate the practical effect of the developed ZG electrolyte additive, full cells with $NH_4V_4O_{10}$ (NVO) as the cathode were assembled for subsequent electrochemical tests. For the synthesized cathode sample, Fig. S10 shows the conducted XRD result that indicates the main component should
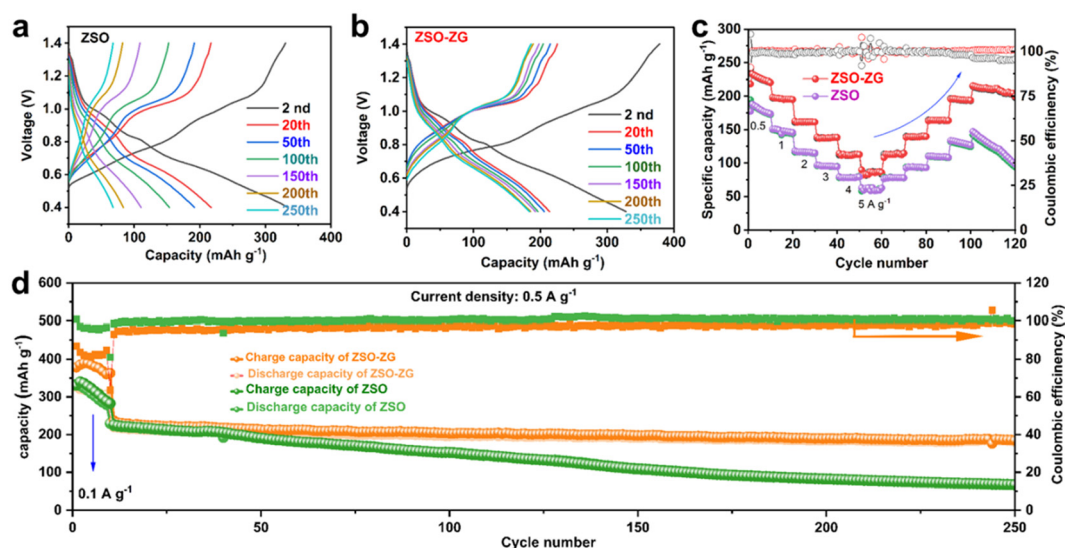

Fig. 5 Discharge–charge profiles of the full cells with (a) ZSO and (b) ZSO–ZG electrolytes. (c) Rate capabilities. (d) Long-term cycling performances of the full cells using different electrolytes at a current density of 0.5 A g^{-1}.

be confirmed as $NH_4V_4O_{10}$ (PDF#31-0075), which is well consistent with the reported work.[53] Moreover, the related SEM image of the successfully prepared material is depicted in Fig. S11, from which the typical morphology of a uniform nanobelt can be observed. As illustrated in Fig. 5a and b, the specific discharge–charge curves of full cells with two electrolytes in different cycles show that ZG introduction significantly improves cycling stability during the long-term process and effectively slows down capacity decay. Fig. 5c further displays the rate performance of these two full cells at different current densities of 0.5, 1, 2, 3, 4 and 5 A g^{-1}. It can be observed that the cell using ZSO–ZG exhibits higher capacity delivery than the cell with ZSO and maintains a more delayed capacity decay after severe activation at large current densities. To explore the long-term electrochemical stability of two electrolytes in full cells, charge/discharge processes at a current density of 0.5 A g^{-1} have been measured, as illustrated in Fig. 5d. Specifically, the full cell with ZSO–ZG can still perform more excellent capacity retention and larger specific capacities during the whole 250 cycles. There is a superior initial capacity delivery of 226.3 mAh g^{-1}; then, the specific capacity of 184.5 mAh g^{-1} can be maintained after 250 cycles, corresponding to a capacity retention of 81.5%. However, for the cell with ZSO electrolyte, a rapid capacity loss occurs only after 8 cycles, and a low capacity of 67 mAh g^{-1} is achieved at the 250th cycle (capacity retention of 29.6%). Therefore, the ZG additive helps improve decay behavior in the capacity delivery of AZIBs.

3. Conclusion

In this study, ZG is explored as a functional electrolyte additive of AZIBs for improving electrochemical performance. Improved activation energy, homogenized dispersion of zinc ions and increased ion transference number are well achieved in the electrolyte with ZG. Moreover, owing to the unique structure of rich hydroxyl groups in the ZG additive, preferential adsorption on the zinc interface can effectively relieve the HER caused by free water and achieve the effective alleviation of corrosion by-products. Abundant zincophilic sites provided by the ZG additive can induce dispersed zinc distribution and growth, thereby preventing dendrite formation. When applied in assembled cells, prolonged cycling lifespan (3200 h), superior rate performance (up to 10 mA cm^{-2}), ultrahigh CE performance (99.8%), small voltage polarization (65.0 mV for 400 cycles) and superior capacity retention (81.5% after 250 cycles) can be delivered in electrolyte using ZG. This electrolyte modification strategy plays a helpful role in improving the cycle stability and reversibility of AZIBs and can provide significant guidance for developing functional electrolytes toward long-life, stable and high-performance energy storages systems.

Conflicts of interest

There are no conflicts to declare.

Data availability

The data supporting this article have been included as part of the main manuscript and its supplementary information. Supplementary information is available. See DOI: https://doi.org/10.1039/d5dt02192h.

Acknowledgements

References

1 J. Zhang, *et al.*, Energy Storage Mechanisms of Anode Materials for Potassium Ion Batteries, *Mater. Today Energy*, 2021, **21**, 100747.

2 L. T. Hu, *et al.*, The Rising Zinc Anodes for High-energy Aqueous Batteries, *Energy Chem.*, 2021, **3**(2), 100052.

3 B. Liu, *et al.*, Safety Issues and Mechanisms of Lithium-Ion Battery Cell Upon Mechanical Abusive Loading: a Review, *Energy Storage Mater.*, 2020, **24**, 85–112.

4 B. Tang, *et al.*, Issues and Opportunities Facing Aqueous Zinc-Ion Batteries, *Energy Environ. Sci.*, 2019, **12**(11), 3288–3304.

5 T. C. Li, *et al.*, Recent Progress in Aqueous Zinc-Ion Batteries: a Deep Insight into Zinc Metal Anodes, *J. Mater. Chem. A*, 2021, **9**(10), 6013–6028.

6 S. Chen, *et al.*, Enabling Low-Temperature and High-Rate Zn Metal Batteries by Activating Zn Nucleation with Single-Atomic Sites, *ACS Energy Lett.*, 2022, **7**(11), 4028–4035.

7 Y. Li, *et al.*, Designing Advanced Aqueous Zinc-Ion Batteries: Principles, Strategies, and Perspectives, *Energy Environ. Mater.*, 2022, **5**(3), 823–851.

8 Y. W. Cui, *et al.*, Challenges, Strategies, and Perspectives of Anode Protection in Aqueous Zinc-Ion Batteries, *ACS Mater. Lett.*, 2024, **6**(2), 611–626.

9 C. H. Nie, *et al.*, Recent Progress on Zn Anodes for Advanced Aqueous Zinc-Ion Batteries, *Adv. Energy Mater.*, 2023, **13**(28), 2300606.

10 P. Kulkarni, *et al.*, Chemical Surface Tuning of Zinc Metal Anode Toward Stable, Dendrite-Less Aqueous Zinc-Ion Batteries, *J. Energy Chem.*, 2023, **86**, 1–8.

11 H. W. Liu, *et al.*, Interface Challenges and Optimization Strategies for Aqueous Zinc-Ion Batteries, *J. Energy Chem.*, 2023, **77**, 642–659.

12 Q. Li, *et al.*, Dendrites Issues and Advances in Zn Anode for Aqueous Rechargeable Zn-based Batteries, *EcoMat*, 2020, **2**, e12035.

13 J. P. Chen, *et al.*, Challenges and Perspectives of Hydrogen Evolution-Free Aqueous Zn-Ion Batteries, *Energy Storage Mater.*, 2023, **59**, 102767.

14 X. Chen, *et al.*, On Energy Storage Chemistry of Aqueous Zn-Ion Batteries: From Cathode to Anode, *Electrochem. Energy Rev.*, 2023, **6**, 33–121.

15 S. N. Yang, *et al.*, Advances in the Structure Design of Substrate Materials for Zinc Anode of Aqueous Zinc Ion Batteries, *Green Energy Environ.*, 2023, **8**(6), 1531–1552.

16 X. F. Chen, *et al.*, Hexagonal WO$_3$/3D Porous Graphene as a Novel Zinc Intercalation Anode for Aqueous Zinc-Ion Batteries, *ACS Appl. Mater. Interfaces*, 2022, **14**(3), 3961–3969.

17 Y. H. Lin, *et al.*, Binder-Free Freestanding 3D Zn-Graphene Anode Induced from Commercial Zinc Powders and Graphene Oxide for Zinc Ion Battery with High Utilization Rate, *ACS Appl. Energy Mater.*, 2022, **5**(12), 15222–15232.

18 T. C. Liu, *et al.*, Zincophilic Sn Sites Induced the Local Ion Enrichment for Compact and Homogenous Growth of Zn Biscuits in Long-life Zn Metal Batteries, *J. Mater. Chem. A*, 2024, **12**(4), 2283–2293.

19 C. C. Fan, *et al.*, Stratified Adsorption Strategy Facilitates Highly Stable Dendrite Free Zinc Metal Anode, *Energy Storage Mater.*, 2023, **56**, 468–477.

20 Y. M. Chen, *et al.*, Ultrathin Zincophilic Interphase Regulated Electric Double Layer Enabling Highly Stable Aqueous Zinc-Ion Batteries, *Nano-Micro Lett.*, 2024, **16**, 96–110.

21 P. Wu, *et al.*, An Industrially Applicable Passivation Strategy for Significantly Improving Cyclability of Zinc Metal Anodes in Aqueous Batteries, *Adv. Mater.*, 2024, **36**(2), 2306601.

22 X. M. Ye, *et al.*, Imide-Pillared Covalent Organic Framework Protective Films as Stable Zinc Ion-Conducting Interphases for Dendrite-Free Zn Metal Anodes, *J. Energy Chem.*, 2024, **97**(2), 470–477.

23 Z. L. Cai, *et al.*, Sandwich-Structured Double-Sided Hydrophobic Diaphragm for Long-Life Zinc Ion Batteries, *Chem. Eng. J.*, 2025, **514**, 163120.

24 Y. Zu, *et al.*, Functionalized Separator Strategies toward Advanced Aqueous Zinc-Ion Batteries, *Adv. Energy Mater.*, 2023, **13**(20), 2300403.

25 T. C. Liu, *et al.*, Uniform Distribution of Zinc Ions Achieved by Functional Supramolecules for Stable Zinc Metal Anode with Long Cycling Lifespan, *Energy Storage Mater.*, 2022, **45**, 1074–1083.

26 Y. F. Geng, *et al.*, Electrolyte Additive Engineering for Aqueous Zn Ion Batteries, *Energy Storage Mater.*, 2022, **51**, 733–755.

27 L. L. Zheng, *et al.*, Competitive Solvation-Induced Interphases Enable Highly Reversible Zn Anodes, *ACS Energy Lett.*, 2023, **8**(5), 2086–2096.

28 H. Y. Lu, *et al.*, Multi-Component Crosslinked Hydrogel Electrolyte toward Dendrite-Free Aqueous Zn Ion Batteries with High Temperature Adaptability, *Adv. Funct. Mater.*, 2022, **32**(19), 2112540.

29 S. Guo, *et al.*, Fundamentals and Perspectives of Electrolyte Additives for Aqueous Zinc-Ion Batteries, *Energy Storage Mater.*, 2021, **34**, 545–562.

30 X. M. Xiao, *et al.*, Trace Small Molecular/Nano-Colloidal Multiscale Electrolyte Additives Enable Ultra-Long Lifespan of Zinc Metal Anodes, *Adv. Mater.*, 2024, **36**(38), 2408706.

31 S. Q. Xu, *et al.*, Electrolyte and Additive Engineering for Zn Anode Interfacial Regulation in Aqueous Zinc Batteries, *Small Methods*, 2024, **8**(6), 2300268.

32 X. N. Zhu, *et al.*, Recent Advances in Electrolyte Additives for Aqueous Zn Metal Batteries: Functional Mechanisms, Interfacial Engineering, and Dendrite Suppression Strategies, *Small*, 2025, **8**(6), 2300268.

33 T. C. Liu, *et al.*, Bifunctional Interface Stabilizer for Promoting Preferential Crystal Face Adsorption and Inducing Planar Zn Growth, *J. Mater. Chem. A*, 2024, **12**(39), 26536–26543.

34 B. J. Wang, *et al.*, Synergistic Solvation and Interface Regulations of Eco-Friendly Silk Peptide Additive Enabling Stable Aqueous Zinc-Ion Batteries, *Adv. Funct. Mater.*, 2022, **32**(23), 2112693.

35 G. Ni, *et al.*, A Multifunctional Phenylalanine Additive Stabilizing Zinc Anodes in Aqueous Zinc Ion Batteries, *J. Mater. Chem. A*, 2024, **12**(11), 6610–6622.

36 D. M. Xu, *et al.*, Chelating Additive Regulating Zn-Ion Solvation Chemistry for Highly Efficient Aqueous Zinc-Metal Battery, *Angew. Chem., Int. Ed.*, 2024, **63**(21), e202402833.

37 C. Huang, *et al.*, Highly Reversible Zinc Metal Anodes Enabled by Protonated Melamine, *J. Mater. Chem. A*, 2022, **10**(12), 6636–6640.

38 Y. H. Quan, *et al.*, Electrolyte Additive of Sorbitol Rendering Aqueous Zinc-Ion Batteries with Dendrite-free Behavior and Good Anti-freezing Ability, *Chem. Eng. J.*, 2023, **458**, 141392.

39 H. Z. Wang, *et al.*, Nicotinic Acid Additive with a Double Regulating Mechanism for High-Performance Aqueous Zinc Ion Batteries, *J. Mater. Chem. A*, 2024, **12**(11), 6376–6386.

40 Z. C. Tian, *et al.*, Ethanol as Solvent Additives with Competitive Effect for High-Stable Aqueous Zinc Batteries, *ACS Appl. Mater. Interfaces*, 2024, **16**(17), 21857–21867.

41 Q. Guo, *et al.*, A Preferentially Adsorbed Layer on the Zn Surface Manipulating Ion Distribution for Stable Zn Metal Anodes, *Energy Environ. Sci.*, 2024, **17**(8), 2888–2896.

42 X. M. Huang, *et al.*, Critical Triple Roles of Sodium Iodide in Tailoring the Solventized Structure, Anode-Electrolyte Interface and Crystal Plane Growth to Achieve Highly Reversible Zinc Anodes for Aqueous Zinc-Ion Batteries, *J. Colloid Interface Sci.*, 2023, **650**, 875–882.

43 W. J. Feng, *et al.*, Dendrite-free Zinc Metal Anodes Enabled by Electrolyte Additive for High-Performing Aqueous Zinc-Ion Batteries, *Dalton Trans.*, 2023, **52**(22), 7457–7463.

44 W. H. Ding, *et al.*, Revolutionizing Aqueous Zn-ion Batteries: Precision Control of H$_2$O Activity and Zn Deposition through Ammonium Oxalate Additive, *Chem. Eng. J.*, 2024, **481**, 148544.

45 H. Y. Wu, *et al.*, Tailoring the Interfacial Electric Field Using Silicon Nanoparticles for Stable Zinc-ion Batteries, *Adv. Funct. Mater.*, 2024, **34**(5), 2213882.

46 X. J. Gong, *et al.*, Inhibiting Dendrites on Zn Anode by ZIF-8 as Solid Electrolyte Additive for Aqueous Zinc Ion Battery, *Colloids Surf.*, 2023, **656**, 130255.

47 Y. J. Zhang, *et al.*, 2D Anionic Nanosheet Additive for Stable Zn Metal Anodes in Aqueous Electrolyte, *Chem. Eng. J.*, 2022, **430**, 133042.

48 W. H. Li, *et al.*, Electric-Responded 2D Black Phosphorus Nanosheets Induce Uniform Zn^{2+} Deposition for Efficient Aqueous Zinc-Metal Batteries, *Adv. Funct. Mater.*, 2024, **34**(41), 2404146.

49 K. K. Bao, *et al.*, Construction of Low Dielectric Aqueous Electrolyte with Ethanol for Highly Stable Zn Anode, *Nano Energy*, 2024, **120**, 109089.

50 M. K. Su, *et al.*, Multisite Cooperative Regulation of Solvation and Interface via Dynamic Additive Engineering for Highly Reversible Zinc Batteries, *Angew. Chem., Int. Ed.*, 2025, e202511685.

51 C. Huang, *et al.*, Amphoteric Polymer Strategy with Buffer-Adsorption Mechanism for Long-Life Aqueous Zinc Ion Batteries, *Adv. Funct. Mater.*, 2024, **34**(26), 2315855.

52 T. A. Nigatu, *et al.*, Synergetic Effect of Water-in-Bisalt Electrolyte and Hydrogen-Bond Rich Additive Improving the Performance of Aqueous Batteries, *J. Power Sources*, 2021, **511**, 230413.

53 B. Y. Tang, *et al.*, Engineering the Interplanar Spacing of Ammonium Vanadates as a High-performance Aqueous Zinc-ion Battery Cathode, *J. Mater. Chem. A*, 2019, 7(3), 940–945.